DOI: 10.61782/fa.2023.0032

forum acusticum 2023

FINITE ELEMENT MODELLING AND OPTIMISATION OF MULTI-MATERIAL ACOUSTIC BLACK HOLES

Beth Austin[1*] **Jordan Cheer**[1]
[1] Institute of Sound and Vibration Research, University of Southampton, Southampton, United Kingdom

ABSTRACT

Geometric acoustic black holes (ABHs) have been proven to be effective as a lightweight passive vibration control solution. However, the thin geometries associated with the design leaves them susceptible to damage. Multi-material ABHs have been proposed as an alternative, whereby the material properties and hence the acoustic impedance of the structure varies along the direction of wave travel as opposed to the geometry. Multi-material ABHs are produced through multi-material additive manufacturing, a relatively costly process which produces final components that cannot easily be altered after production. As such, an accurate numerical model is required to design and optimise the multi-material ABH configuration. This work investigates the best practices for finite element modelling and optimisation of a multi-material ABH design in a beam termination application. Considerations are made into accuracy, computational cost, and the potential effects of the additive manufacturing process on the effective material properties.

Keywords: *Acoustic black holes, additive manufacturing, finite element modelling*

1. INTRODUCTION

Acoustic black holes, as first theorised by Mironov in 1988 [1], have rapidly expanded as an area of interest. Since the first practically realisable ABH was realised by Krylov et al [2], development of so-called geometric ABHs has continued and now includes a broad range of ABH designs [3–5]. One major benefit of an ABH is that the reduction in structural vibration can be realised without adding material and hence mass to the structure and as such is useful in applications where the overall mass of the system is a concern.

One common problem that geometric ABH designs experience is damage due to the thin sections inherent to the design. A reduction in thickness is used to reduce wavespeed, resulting in a greater proportion of wave energy dissipation. This thin, free-moving edge leaves the structure susceptible to damage through both impact and fatigue [6]. However, a similar reduction in wavespeed can be achieved through varying the effective material properties in the direction of wave travel, while maintaining a constant external geometry. Ideally, this would be a smooth, gradual variation in impedance and several possible methods have been proposed to achieve this [7, 8]. A potentially easier solution would be the multi-material ABH (MM-ABH), where discrete sections of materials would be used in order to approximate the desired gradient of material properties. This paper discusses suitable methods for modelling and optimising the design of a MM-ABH in a beam termination application.

Section 2 of this paper discusses the current geometric ABH theory and suggested multi-material ABH configurations. Section 3 discusses numerical modelling and optimisation methods of a multi-material ABH. Section 4 discusses the performance of the optimised configuration. Section 5 outlines the current position of the investigations and considers future work.

*__Corresponding author__: b.austin@soton.ac.uk.

2. ABH BEAM TERMINATIONS

2.1 Geometric ABH

An ABH is realised by varying the geometry along the direction of wave travel to cause a reduction in wavespeed. In a beam termination application, the wavespeed along the ABH taper can be expressed as [2, 9]

$$c_\omega(x,\omega) = \left(\frac{E(x)h(x)^2\omega^2}{12\rho(x)}\right) \tag{1}$$

where c_f is the wavespeed at a given frequency, x is the coordinate position along the beam, E is the Young's modulus, h is the height of the beam, ω is the angular frequency of oscillation, and ρ is the density. As seen in Eq. 1, wavespeed is proportional to the square of the beam height. In a geometric ABH, the height typically follows a power law profile given by

$$h(x) = (h_0 - h_{tip})\left(\frac{l_{ABH} - x}{l_{ABH}}\right)^\mu + h_{tip} \tag{2}$$

where l_{ABH} is the length of the ABH taper, x is the position along the taper with $x = 0$ at the junction between the beam and ABH, h_0 is the height of the uniform beam section, and h_{tip} is the height of the ABH tip. This power law profile provides a gradual reduction in acoustic impedance and thus wavespeed, without the wave reflections typically found at impedance change boundaries.

Ideally, the taper would have a tip height of zero, but this cannot be practically manufactured. Instead, the taper is truncated with a finite tip height, h_{tip}, thus preventing total dissipation of wave energy and causing some wave energy to be reflected back into the beam. To reduce the resulting reflected wave, a layer of damping material is typically added to the surface of the ABH, as can be seen in Fig. 1. This dissipates the wave energy in the taper, mitigating the effect of the wave reflection.

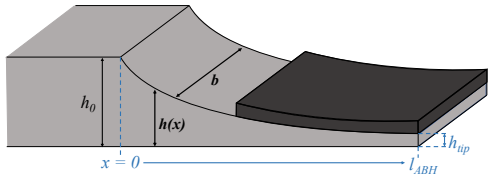

Figure 1. Geometric ABH with damping layer

Acoustic black holes are only effective above a certain frequency, the so-called cut-on frequency, as defined by [10]

$$\omega_{cut-on} = \frac{h_0}{2\pi l_{ABH}^2}\sqrt{\frac{E(40-24\nu)}{12\rho(1-\nu^2)}} \tag{3}$$

where ν is the Poisson's ratio of the material. Below this frequency, the ABH provides no significant vibration reduction effect. The cut-on frequency coincides with the first bending mode of the ABH taper and as such, the effective range of the ABH can be changed by altering the length of the ABH taper.

2.2 Graded Material Property ABH

As discussed in Section 1, a similar reduction of wavespeed can be achieved by decreasing the Young's modulus along the length of the beam. To match the behaviour of a geometric power law profile, the Young's modulus in the graded material ABH should follow the profile given by

$$E(x) = \left(\frac{h(x)^2}{h_0^2}\right)E_0 \tag{4}$$

where E_0 is the Young's modulus of the beam section and $h(x)$ is the height profile of the equivalent geometric ABH referred to in Eq 2. The realisation of this profile would require a continuously varying Young's modulus along the length of the beam and would also assume constant density and damping effects as Young's modulus is varied.

It is difficult to achieve a continuous gradient of material properties and as such the multi-material ABH uses discrete sections of a pre-selected range of materials, as seen in Fig. 2. The section lengths are then optimised based on a criterion of ABH performance, usually reflection coefficient or kinetic energy in the beam section. This design could then be produced using multi-material additive manufacture or another suitable material layering procedure.

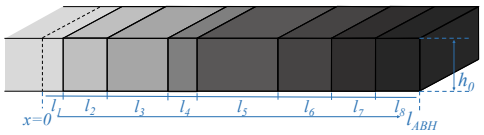

Figure 2. Multi-material ABH in beam termination application

For this investigation, a range of 8 materials from the Stratasys digital materials line has been chosen, Their

Young's modulus and loss factor are listed in Table 1. The density is consistent across materials at $\rho = 1160kg/m^3$ for all materials used. The Stratasys digital materials are designed to be used together in multi-material inkjet printing applications which is why they were chosen for this investigation.

Table 1. Material properties of Stratasys digital materials

Material	$E(GPa)$	η
VeroClear	2.347	0.0609
RGD8710	2.068	0.0677
RGD8720	1.905	0.0729
RGD8730	1.589	0.1154
FLX9095	0.0708	0.4524
FLX9070	0.0046	0.7386
FLX9050	0.0016	0.9722
Tango+	0.0006	1.0512

3. NUMERICAL MODELLING

3.1 ABH models

Previous investigations into modelling and optimising multi-material ABHs has been performed [11]. This previous work used a 1D COMSOL finite element model of the MM-ABH using the beam physics module. Whilst this method is beneficial in terms of computational costs, the 1D model does not fully characterise the behaviour of the design. The beam physics assumptions are only valid at sufficiently low frequencies when no cross-body modes of the system are excited. With the range of materials used in this investigation, cross-body and torsional modes will occur at relatively low frequencies. As such, a 1D beam model would not be sufficient.

For the purposes of this investigation, a 2D model of a multi-material ABH was implemented in COMSOL using the plate mechanics physics module. The model consisted of an 18cm uniform VeroClear beam with a 7 cm MM-ABH termination. The overall external dimensions were $25\times4\times1$ cm. Initially, equal section lengths of each material were used, with material Young's modulus decreasing along the beam. The model was meshed with free triangular elements with a maximum element size equivalent to 10 elements per wavelength at 10 kHz for each material section, since this is the finest mesh resolution required across the frequency range investigated.

The model was excited with an edge load of 1 N at frequencies of 20 Hz - 10 kHz at 20 Hz intervals. the load was applied at the opposite end to the MM-ABH termination. All remaining boundaries were assumed to be free. The model was subject to the following equation, solved in the frequency domain and discretized with quadratic elements.

$$\begin{aligned} -\rho\left(\omega^2\mathbf{u} + z\omega^2\mathbf{ar}\right) \\ = \nabla\cdot s + \mathbf{F}_v e^{i\Phi} + 6\left(\mathbf{M}_v\times\mathbf{n}\right)\frac{z}{d}e^{i\tilde{\Phi}} \\ \sigma_z = 0, -1\leq z\leq 1 \end{aligned} \tag{5}$$

In this equation, $\boldsymbol{u}$ and $\boldsymbol{a}$ are the displacement and rotational displacement vectors, $\boldsymbol{r}$ is the undeformed mid surface position, $\boldsymbol{F_v}$ and $\boldsymbol{M_v}$ are the force and moment vectors respectively, and $\boldsymbol{n}$ is the normal to the surface in the deformed state.

To provide a comparison, a 2D model of a geometric ABH was also implemented using the solid mechanics module. The ABH configuration had $l_{ABH} = 7$ cm, to remain consist with the optimised MM-ABH, and followed a power law as outlined in Eq. 2 with $h_{tip} = 0.5$ mm and $\mu = 4$. This profile was chosen as it is a well-studied configuration that provides a suitable ABH effect [9, 12]. The uniform beam and ABH were made of VeroClear. A damping layer of Tango+ was added to the surface of the ABH, extending over 6 cm of the ABH with a layer thickness of 4 mm. A separate 2D model of a uniform VeroClear beam was also implemented to show the improvements in performance achievable through both ABH configurations.

3.2 Section length optimisation

An optimisation routine was implemented to find the section lengths of each material in the ABH termination which provide the lowest average kinetic energy in the beam across frequency. The section lengths were constrained such that the sum of the lengths is always equal to 7 cm. The model also requires that all 8 materials are used in the ABH and must appear in order of decreasing Young's modulus with a layer thickness of at least 0.1 mm. This minimum layer thickness was required as the model would not rebuild itself during the optimisation should an

individual layer thickness be reduced to zero. Introducing these constraints also reduces the optimisation space.

This constrained, non-linear optimisation problem was solved using the MATLAB multi-start routine with the fmincon solver [13]. This routine uses a gradient descent algorithm to find a local minimum. This process is repeated for a total of 10 start points, including the equal section lengths outlined in Section 3.1 and an additional 9 random start points. This maximises the chances of finding a global minimum.

4. DISCUSSION

The optimised section lengths of each material are listed in Table 2. The optimisation routine clearly favours the softer materials used in the design, as evidenced by the much larger sections of these materials in the MM-ABH design. This is likely due to the higher loss factor and thus greater ability to dissipate energy of these materials. It could be inferred that the optimisation routine would prefer to remove the four most rigid materials given how small the section lengths are. However, each is larger than the minimum section length of 0.1mm suggesting that having a small amount of each of these materials is beneficial. The inclusion of these materials reduces the changes in acoustic impedance at each material boundary thus allowing a greater proportion of wave energy to reach the highly damped materials at the end of the ABH termination, and allowing a greater dissipation of energy in the ABH.

Table 2. Section lengths of each material in the optimised MM-ABH

Material	Length, mm
VeroClear	0.6
RGD8710	0.7
RGD8720	0.8
RGD8730	0.9
RGD9095	10.7
RGD9070	3.1
RGD9050	25.9
Tango+	27.3

Figure 3 shows the kinetic energy of the 18cm long uniform beam section of the optimised MM-ABH, a geometric ABH, and a 25 cm uniform beam made of VeroClear. The position of the peaks are shifted to higher frequencies in the beams with ABHs, due to the effective shortening of the uniform beam section. The equivalent peaks from the ABH beams are also damped as compared to the uniform beam due to the inclusion of materials with higher loss factors, as detailed in Table 1. At all frequencies, the kinetic energy of the ABH terminated beams is significantly lower than that of the uniform beam.

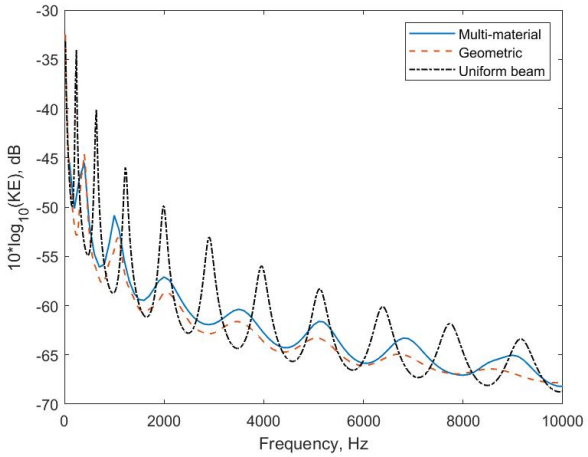

Figure 3. Predicted kinetic energy of uniform beam section of a MM-ABH (blue solid), geometric ABH (red dashed), and uniform beam without ABH termination (black dot-dash)

A more significant reduction in kinetic energy is seen at low frequencies than at high frequencies. The first bending mode experiences a reduction in kinetic energy of 10 dB as compared to a reduction of around 2 dB at the highest order mode shown. Since the optimisation routine reduces mean kinetic energy, it follows that most reduction on kinetic energy will occur at lower frequencies where the kinetic energy of the untreated beam is significantly higher. Reduction of kinetic energy at low frequencies will have a more significant impact on the mean kinetic energy value.

Equation 3 provides an estimation of the minimum effective frequency of an ABH. The Poisson's ratio of the materials used is unknown and as such an estimation is used based on the Poisson's ratio of acrylic, the material that VeroClear is designed to simulate [14]. Using a Poisson's ratio of $\nu = 0.35$, the cut-on frequency of the geo-

metric ABH is approximately 800 Hz. It is assumed that the MM-ABH will have a similar cut-on frequency since the length of the ABHs is consistent. The first peak in the ABH beam kinetic energy profiles occurs below this frequency, at roughly 400 Hz, and a significant reduction in kinetic energy magnitude of around 10 dB can be seen compared to the first peak in the uniform beam profile. This reduction is likely due to the significant amount of damping material added to the structure as opposed to any ABH effect.

Performance between the geometric and MM-ABH is comparable at the first bending mode, as seen in Figure 4, however this performance diverges at higher frequencies with the geometric ABH out-performing the MM-ABH. It is likely that the sudden change in impedance at the material boundaries in the MM-ABH, and subsequent reflection of wave energy, is the cause of this discrepancy. The gradual impedance change in the geometric ABH limits the reflected proportion of wave energy as compared to the MM-ABH, causing a greater proportion of energy to be dissipated in the taper. It may be the case that during manufacture, there will be some blending of materials at material boundaries and as such, there will not be the predicted sudden change in impedance. This will require production and testing of a MM-ABH of this configuration.

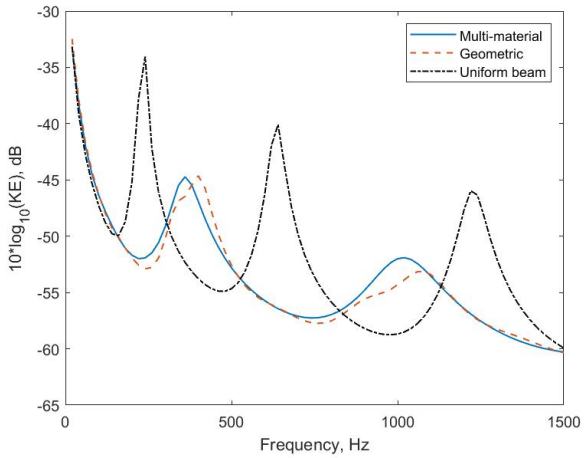

Figure 4. Low frequency kinetic energy behaviour of uniform beam section of three ABH termination configurations

It is also possible that the material properties outlined in the COMSOL model are not accurate to the physical materials. Modelling practices for multi-material additively manufactured structures are still under investigation as the manufacturing methods impact the effective material properties that are not consistently predictable, such as material blending during printing [15]. Moreover, polymers often have frequency dependent material properties at higher frequencies. The models in this investigation consider the materials used to be homogeneous, isotropic, and frequency independent in nature. As such, when compared to measurements of a physical prototype, there may be discrepancies between the model and physical system that could be accounted for by these differences in material properties.

Regardless of these differences, the MM-ABH still provides a significant reduction in kinetic energy of the beam across frequency. If predictions are correct that the MM-ABH configuration is less susceptible to damage due to the uniform external dimensions, this slight reduction in vibration control performance may be seen as a necessary trade-off for use in real-world application.

5. CONCLUSIONS

The work presented in this paper considered the best practices for modelling and optimising a MM-ABH in a beam termination application. Simulations suggest that it is possible to produce an effective vibration control solution comparable to a geometric ABH by optimising section lengths of different materials to form such a MM-ABH. When compared to an untreated beam, significant reductions in kinetic energy are observed.

Further investigation is required into the materials used to better inform the modelling practices of polymer MM-ABHs in addition to validation of these models through testing of physical prototypes. Additional investigation into the resistance of a MM-ABH to damage and fatigue compared to a geometric ABH is also required. Should this expected increase in fatigue life be possible, use in application as a waveguide should be considered, such as automotive and transportation vibrations.

Future investigations should consider material order in addition to whether all materials are required in the MM-ABH. This would require a more complex finite element model and optimisation routine due to the model rebuild routine that would need implementing, thus increasing computational cost. However, the small section lengths of some materials in this optimisation suggest this would be a worthwhile area of investigation to confirm

whether or not such a broad range of materials is required.

6. ACKNOWLEDGMENTS

This work was supported by an EPSRC Prosperity Partnership (No. EP/S03661X/1). The authors acknowledge the use of IRIDIS High Performance Computing Facility and associated support services at the University of Southampton in the completion of this work. Thanks to Dr Anil Bastola at the Centre for Additive Manufacturing at the University of Nottingham for their investigations into the materials used.

7. REFERENCES

[1] M. A. Mironov, "Propagation of a flexural wave in a plate whose thickness decreases smoothly to zero in a finite interval," *Soviet Physics Acoustics-Ussr*, vol. 34, no. 3, pp. 318–319, 1988.

[2] V. V. Krylov and F. J. Tilman, "Acoustic 'black holes' for flexural waves as effective vibration dampers," *Journal of Sound and Vibration*, vol. 274, pp. 605–619, jul 2004.

[3] M. X. He and Q. Ding, "Data-driven optimization of the periodic beam with multiple acoustic black holes," *Journal of Sound and Vibration*, vol. 493, p. 115816, feb 2021.

[4] J. Y. Lee and W. Jeon, "Vibration damping using a spiral acoustic black hole," *The Journal of the Acoustical Society of America*, vol. 141, p. 1437, mar 2017.

[5] J. Cheer, K. Hook, and S. Daley, "Active feedforward control of flexural waves in an Acoustic Black Hole terminated beam," *Smart Materials and Structures*, vol. 30, no. 3, 2021.

[6] A. Keys and J. Cheer, "Fatigue analysis of an acoustic black hole," *28th International Condress on Sound and Vibration*, 2022.

[7] W. Zheng, S. S. He, R. Tang, and S. S. He, "Damping Enhancement Using Axially Functionally Graded Porous Structure Based on Acoustic Black Hole Effect," *Materials 2019, Vol. 12, Page 2480*, vol. 12, p. 2480, aug 2019.

[8] V. Georgiev, J. Cuenca, M. Moleron Bermudez, F. Gautier, and L. Simon, "Recent progress in vibration reduction using Acoustic Black Hole effect," in *10ème Congrès Français d'Acoustique*, 2010.

[9] K. Hook, J. Cheer, and S. Daley, "A parametric study of an acoustic black hole on a beam," *The Journal of the Acoustical Society of America*, vol. 145, no. 6, pp. 3488–3498, 2019.

[10] A. Pelat, F. Gautier, S. C. Conlon, and F. Semperlotti, "The acoustic black hole: A review of theory and applications," *Journal of Sound and Vibration*, vol. 476, p. 115316, jun 2020.

[11] B. Austin, J. Cheer, and A. Bastola, "Design of a multi-material acoustic black hole," in *Internoise 2022*, 2022.

[12] B. Austin and J. Cheer, "Realisation of acoustic black holes using multi-material additive manufacturing," *Frontiers in Physics*, vol. 10, 2022.

[13] R. H. Byrd, J. C. Gilbert, and J. Nocedal, "A trust region method based on interior point techniques for nonlinear programming," *Mathematical Programming*, vol. 89, no. 1, pp. 149–185, 2000.

[14] MatWeb, "Overview of materials for Acrylic, Cast," 2023.

[15] E. Salcedo, D. Baek, A. Berndt, and J. E. Ryu, "Simulation and validation of three dimension functionally graded materials by material jetting," *Additive Manufacturing*, vol. 22, no. May, pp. 351–359, 2018.